Additive Manufacturing 19 (2018) 95–103

Contents lists available at ScienceDirect

Additive Manufacturing

journal homepage: www.elsevier.com/locate/addma

Full length article

Enhanced mechanical properties of additively manufactured bulk metallic glasses produced through laser foil printing from continuous sheetmetal feedstock

Punnathat Bordeenithikasem[a], Yiyu Shen[b], Hai-Lung Tsai[b], Douglas C. Hofmann[a,*]

[a] Engineering and Science Directorate, Jet Propulsion Laboratory, California Institute of Technology, Pasadena, CA 91109, United States
[b] Department of Mechanical and Aerospace Engineering, Missouri University of Science and Technology, Rolla, MO 65409, United States

ARTICLE INFO

Article history:
Received 5 October 2017
Received in revised form
18 November 2017
Accepted 19 November 2017
Available online 21 November 2017

Keywords:
Additive manufacturing
Laser foil printing
Bulk metallic glasses
Four-point bending
X-ray diffraction

ABSTRACT

Metal additive manufacturing (AM) is a rapidly growing field aimed to produce high-performance net-shaped parts. Therefore, bulk metallic glasses (BMGs), known for their superlative mechanical properties, are of remarkable interest for integration with AM technology. In this study, we pioneer the utilization of commercially available BMG sheetmetal as feedstock for AM, using laser foil printing (LFP) technology. LFP and traditional casting were used to produce samples for four-point bending and Vickers hardness measurements to rigorously compare the mechanical performance of samples resulting from these two fabrication techniques. Through LFP, fully amorphous BMG samples with dimensions larger than the critical casting thickness of the same master alloy were successfully made, while exhibiting high yield strength and toughness in bending. This work exemplifies a potential method to fabricate high-value BMG commercial parts, like gears or mechanisms, where the parts are conventionally machined after printing, and greatly benefit from utilizing novel materials.

1. Introduction

The development of novel metal parts for demanding applications requires high-performance structural materials. Conventional crystalline metals, such as steel, aluminum and titanium, offer a wide range of mechanical properties that are attractive for metal parts but have inherent limitations due to their dislocation-based plasticity. Bulk metallic glasses (BMGs) are a class of metal alloys described by their non-crystalline, or amorphous, microstructures and have been widely researched for the past three decades due to their unique combinations of mechanical properties and processing potential. BMGs are typically multicomponent metal alloys designed near deep eutectics which can be cooled from above their melting point to below their glass transition temperature at slow enough cooling rates that they can be formed into parts greater than a few millimeters in thickness without crystallization [1–4]. Commonly researched BMGs that have potential for structural applications include Zr-Ti-Cu-Ni-Be [5,6] and Zr-Cu-Ni-Al [7–11]. These alloy systems can be cast into components more than one centimeter in thickness and still form a glass; i.e. they possess a high "glass forming ability (GFA)." BMGs, by virtue of being designed near deep eutectics, have low enough melting temperatures that they could be die-cast repeatedly into steel molds without damaging to the mold. Die-cast BMG parts were created with complex geometries coupled with high strength, high hardness, and high elasticity [12–14]. The focus of the majority of the emerging BMG industry utilized this manufacturing potential to die-cast or injection mold parts for use in consumer products such as golf clubs, electronic cases, and watches [15–17].

As desired parts increase in complexity, producing net-shaped samples with sufficiently high cooling rates required to fully vitrify the BMG becomes increasingly challenging. Thermoplastic forming (TPF) is a method used to shape BMGs into intricate shapes by decoupling the cooling rate requirement from the forming mechanism [16]. However, TPF requires that the BMG possesses a sufficiently high GFA, such that crystallization doesn't occur during the TPF process [16,18], which will dramatically deteriorate the BMG's mechanical properties [19,20]. This drastically limits the number of alloys that can be potentially used for TPF [21].

Metal additive manufacturing (AM) is another method to fabricate complicated parts with high cooling rates [22–24]. Metal AM has recently seen a rapid and widespread growth in both commercial applications and research due to its unique ability to process difficult-to-manufacture metals into exceptionally com-

* Corresponding author.
E-mail address: dch@jpl.nasa.gov (D.C. Hofmann).

https://doi.org/10.1016/j.addma.2017.11.010
2214-8604/

plex net-shapes [25–29]. While metal AM technologies emerged in the 1990′s [30], little effort was focused on the development of AM technologies for BMGs. Metal AM technology was especially attractive for hard-to-machine metals, such as titanium and steel, but was initially not competitive with easily castable metals, such as aluminum, magnesium, and BMGs. However, as the metal AM technology has matured, part complexity, cost, volume and alloy selection have all improved, allowing many parts to be manufactured into net-shapes that simply could not be manufactured in other ways. Recently, this progress in AM has been extended to BMGs to take advantage of some of the deficiencies in casting.

A number of research groups have therefore starting using commercially available AM machines to fabricate BMG parts. Although many metal AM technologies exist, the vast majority rely on metal feedstock in the form of powder. Manufacturing is then accomplished either through sintering the powder in a bed, called selective laser melting (SLM) or direct metal laser sintering (DMLS), or through depositing the powder into a laser or electron beam melt pool, called direct energy deposition (DED). The availability of BMG powder and equipment for AM makes the technology widely accessible. Laser processing of BMGs has been widely studied [31] and shown to be an effective way to heat the BMG powder to above its liquidus and then rapidly solidify to below the glass transition temperature at cooling rates in the order of 10^3–10^4 K/s [22,24]. The AM technology can be thought of as rapid solidification manufacturing, which is ideally suited for quenching weak glass-forming BMG alloys into amorphous layers. Some groups in the literature have manufactured BMG parts using AM technology from large GFA Zr-based BMGs [32,33] while others have demonstrated weak GFA Fe-based BMGs [23,34]. The imposed cooling rates of AM therefore also broaden the potential alloys that can be manufactured into bulk parts. AM equipment have also been used as a means to scientifically study BMG crystallization [35,36] and for combinatorial evaluation of GFA of BMGs [37,38].

These powder-based systems make up a majority of the metal AM research, however there are a wide assortment of technologies that utilize non-powder-based feedstock, including wire, molten liquid, ribbon, shot, deposition, and metal powder infused with polymeric binders. These feedstock geometries are readily available for BMGs. Fig. 1 demonstrates an assortment of BMG feedstock material that could potentially be used for AM, and Table 1 describes advantages and disadvantages of each. The different BMG feedstock materials listed in Fig. 1 are drawn wire, shot, rods >1 mm, powder, cast plates, wire <1 mm, liquid (an ingot is shown), thin melt-spun ribbon <50 μm thick, and sheetmetal 100–250 μm in thickness. Although not shown here, each BMG feedstock material can be used in one or more specific AM technologies. For example, the Fe-based BMG powder shown in Fig. 1d is suitable for use in commonly available powder-bed AM machines and also for thermal spray AM while the Zr-based ingot in Fig. 1g can be melted in a crucible and then deposited as a liquid stream. The Zr-based BMG shot in Fig. 1b is suitable for metal injection molding (MIM) technology but could also be combined with a polymer binder to do fused deposition modelling (FDM). Ni and Fe-based ribbons in Fig. 1h can fabricated into laminates or fabricated using ultrasonic additive manufacturing (UAM). Rods and wires, like the Zr-based alloys in Fig. 1a,c,f, can be melted and sprayed or deposited as a liquid stream to do AM. Lastly, plates and sheetmetal of BMG, like the Zr-based alloy shown in Fig. 1e,i can be thermoplastically consolidated or laser welded to form net shapes.

To overcome the limitations imposed by powder-based AM technologies, we utilize sheetmetal as a continuous feedstock for AM using laser foil printing (LFP) technology, previously demonstrated in [22,39]. Using LFP and traditional casting, we fabricate samples for measurements of mechanical properties through four-point bending and Vickers hardness, and draw direct comparisons between sample geometry and fabrication method.

2. Experimental

In this study, $Zr_{65}Cu_{17.5}Ni_{10}Al_{7.5}$ amorphous sheetmetal, with a nominal thickness of 150 μm that was manufactured through slow melt spinning using master alloys fabricated from industrial-grade purity constituent elements (produced by Eco FM Co. Ltd., South Korea), was used as feedstock material. The sheetmetal therefore contains nominally 600 ppm of oxygen by weight and 0.25 at.% Hf from the Zr precursor. All LFP experiments were conducted in an Ar-shielded chamber (>99%) using an IPG YLR-1000 CW (continuous wave) fiber laser with a wavelength of 1070 nm and a maximum output power of 1000 W. Prior to the LFP process, the feedstock sheetmetal's surfaces were slightly polished with 800 grit SiC paper followed by ethanol cleaning in order to remove potential surface oxidization. The sheetmetal was pre-fixed on the substrate (and/or previous layer) by laser spots before welding the whole surface to prevent potential sheetmetal deformation. Further details of LFP can be found in our previous publication [22].

For the LFP process, laser power, laser pulse duration, and spot interspacing are the three most important parameters. For successful welding in between layers, the laser power must be sufficiently high such that the weld depth is larger than the sheet thickness. However, above a certain power threshold, the welding mechanism produces a "keyhole" and pores will be generated [40]. Therefore, the laser power must be maintained between the aforementioned limits. The laser pulse duration must be short to avoid crystallization of the amorphous sheetmetal. The size of the fusion zone defines the upper limit of the spot interspacing. If the interspacing is too small, the material may experience multiple reheating and crystallize. If the interspacing is too large, the welding will be discontinuous. Optimizing the laser parameters, samples were fabricated using 300 W laser power in pulse mode, 1 ms laser pulse duration, 430 μm spot size, and 100 μm spot interspacing. Therefore, the resultant pulse energy is 0.3 J/pulse and the power density is 2×10^5 W/cm^2.

LFP samples are fully amorphous, as verified by X-ray diffraction (XRD), and 99.9% dense, measured using the Archimedes principle (Fig. 2). It should be noted that the roughness of laser welded surface was measured as R_a = 2.43 μm. This level of roughness will not affect the laser welding of the next layer. Thus, there is no need to remove the surface irregularities for continuous welding. However, in the presented work, we did polish the welded surface with 800 grit SiC paper followed by ethanol cleaning right before the laser welding, the same protocol as the feedstock sheetmetal, to maintain consistency. Rectangular beams were then printed by LFP on a pure Zr substrate. The beams could then be cut from the substrate using wire electrical discharge machining (EDM). Optical microscopy (OM) was performed on the top and cross sectional views of the sample. The images show evidence of high laser pulse overlap and complete melting in between layers with no contrast produced by crystallinity. Pores are also observed due to "keyholes," which were minimized but could not be avoided due to the thickness and thermal stability of the BMG sheetmetal.

For a comparison of the mechanical properties of samples produced by LFP, sheetmetal from the same batch utilized as feedstock for LFP was carefully remelted, by arc melting, to preserve the composition. The resulting ingots were then suction casted, using the arc melter, into beams that are at least 50 mm long and with 2.5 mm, 3.5 mm, and 4.5 mm square cross sections. XRD was then performed to evaluate GFA of the cast samples.

Oxygen content has been known to deteriorate the GFA and embrittle BMGs of same or similar chemistry to $Zr_{65}Cu_{17.5}Ni_{10}Al_{7.5}$

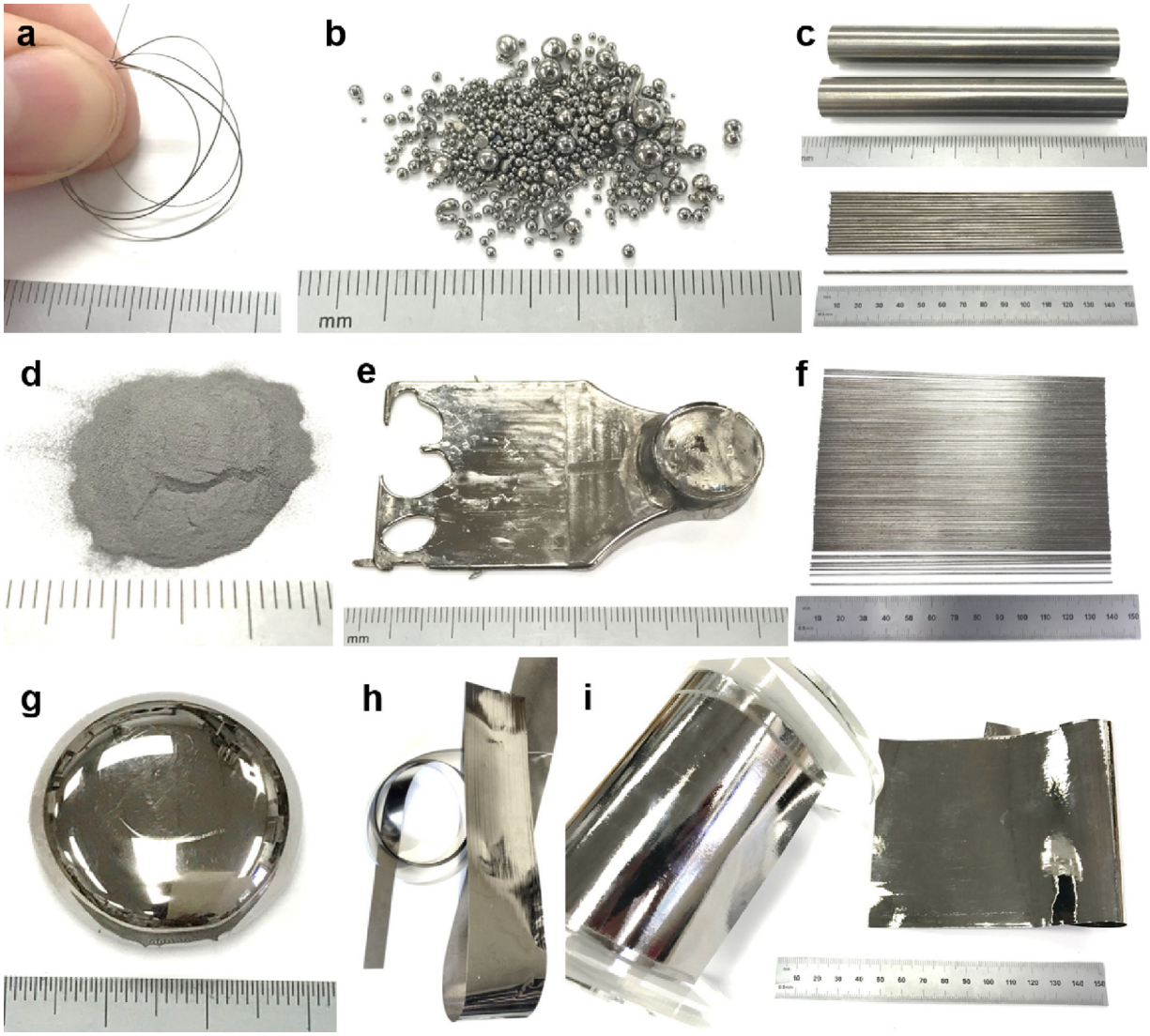

Fig. 1. Examples of BMG feedstock material that can be used for various AM technologies, i.e. (a) wire, (b) pellets, (c) thick cast rods of various diameters, (d) powder, (e) cast plates, (f) thin cast rods, (g) ingot, (h) melt spun ribbon, and (i) melt spun sheetmetal. Smallest divisions on the ruler are 1 mm. Feedstock material produced or acquired by NASA Jet Propulsion Laboratory, California Institute of Technology.

Table 1
Summary of the different BMG feedstock geometries that could be used for AM versus the typical feedstock size, production scalability, relative cost, oxidation and contamination risk, and the overall usefulness for AM.

BMG Feedstock for AM	Typical feedstock size (mm)	Scalable production	Relative cost	Oxidation and Contamination	Usefulness for AM
Drawn Wire	0.3–1	Yes	High	Yes	Low
Spherical shot	0.5–5	Yes	Low	Yes	Low
Large cast rods	2–10	No	High	No	Low
Powder	0.02–0.08	Yes	Low	Yes	High
Cast plates	0.75–5	No	High	No	Low
Thin cast rods	0.5–1	No	High	No	Low
Molten alloy	–	Yes	Low	Yes	High
Melt spun ribbon	0.01–0.05	Yes	Low	No	Low
Sheetmetal	**0.1–1**	**Yes**	**Low**	**No**	**High**

[41–46]. Therefore, to isolate the effect of oxygen content and impurities on the mechanical properties and GFA, laboratory grade samples of $Zr_{65}Cu_{17.5}Ni_{10}Al_{7.5}$ were made using constituent elements of at least 99.99% purity and Zr-crystal bar feedstock free of Hf and with <25 ppm oxygen. The master alloys were first fabricated by arc melting the constituent elements in a Ti-gettered, Ar atmosphere. The ingots were flipped and remelted at least three times to ensure homogeneity. Similarly, the ingots casted into square beams of varying cross section sizes. Cylinders up to 16 mm have been reported in the literature [11], ensuring sufficient GFA to fully vitrify into such geometries. Mechanical tests performed on these beams will serve as the benchmark for the best properties attainable by this alloy composition.

Surface irregularities and flashing on the beams, resulting from the casting or LFP process, were removed by grinding with SiC papers, up to a final 600 grit surface finish. Then, four-point bend-

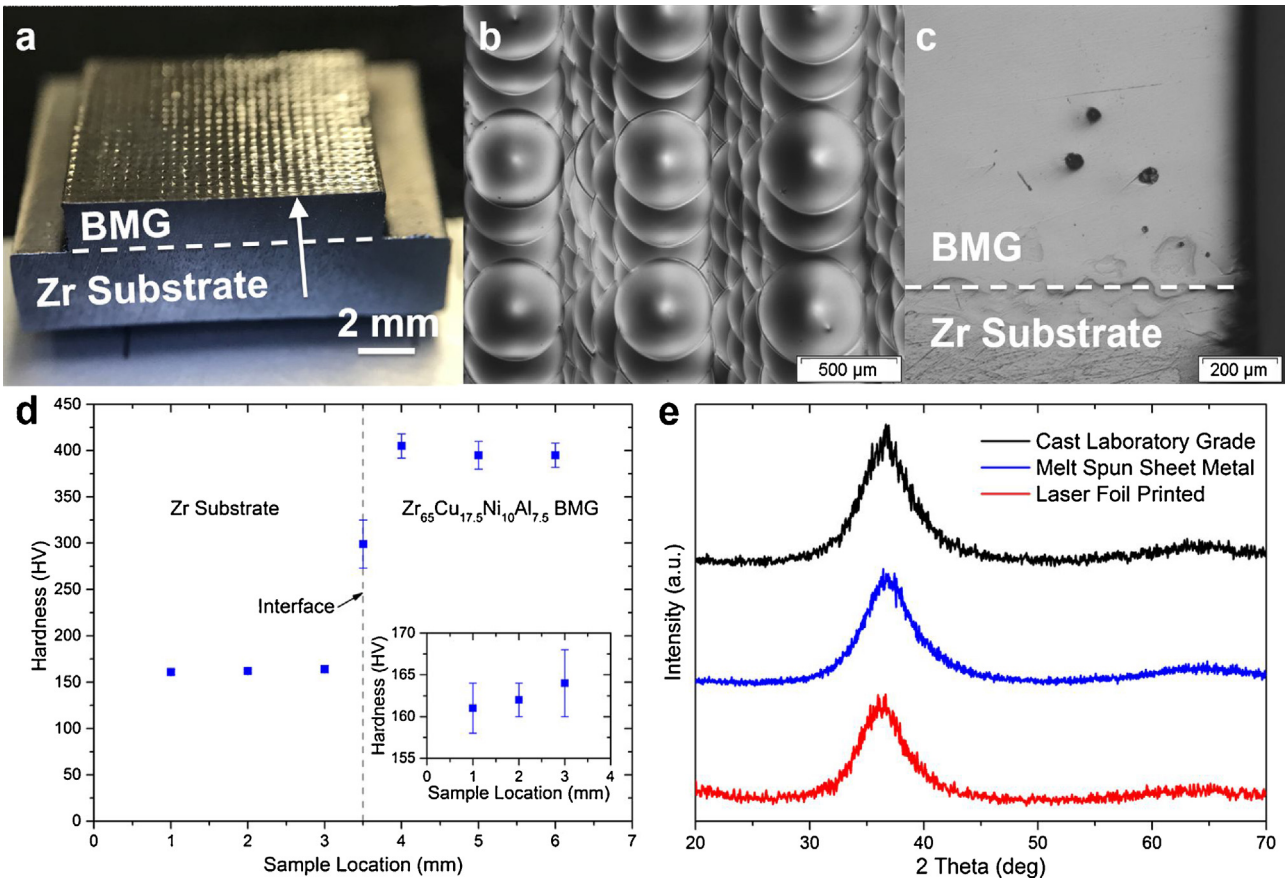

Fig. 2. (a) Cross section of a 2 mm thick LFP sample printed onto a pure Zr substrate. (b) OM image of the top surface of the LFP sample showing the overlap in melting. (c) OM image of the cross sectional view. (d) Vickers hardness along the cross section of the LFP sample starting from the Zr substrate, where "sample location" follows the arrow in (a). (e) XRD measurements of as-cast laboratory grade $Zr_{65}Cu_{17.5}Ni_{10}Al_{7.5}$, the melt spun sheetmetal feedstock, and the LFP sample. The diffuse peaks verify that the samples are amorphous.

ing experiments and Vickers hardness measurements were carried out to evaluate and compare the mechanical properties of samples of various dimensions and fabrication history. A flowchart summarizing the entire experimental process is depicted in Fig. 3.

3. Results and discussion

As seen from Fig. 2, LFP was able to produce fully amorphous samples. Vickers hardness was measured along the cross section in the LFP build direction. The hardness values show a distinct

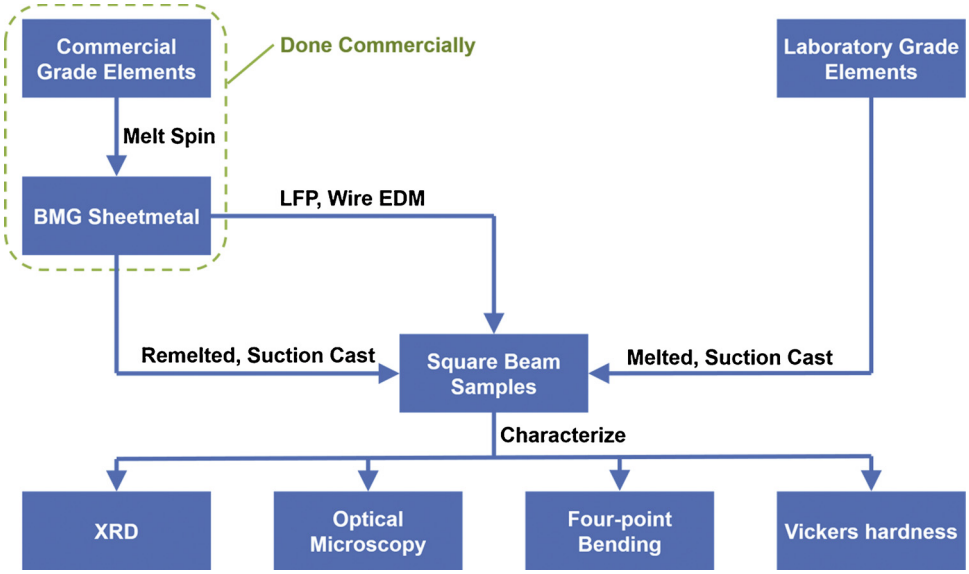

Fig. 3. Flowchart explaining the experimental process for this work.

Table 2
The Vickers hardness values as measured using variable forces with a constant dwell time of 10 s for samples of $Zr_{65}Cu_{17.5}Ni_{10}Al_{7.5}$ with different purities and processing history.

	150 μm Melt Spun $Zr_{65}Cu_{17.5}Ni_{10}Al_{7.5}$ Sheetmetal	2 mm Laser Foil Printed $Zr_{65}Cu_{17.5}Ni_{10}Al_{7.5}$	2 mm Cast Laboratory Grade $Zr_{65}Cu_{17.5}Ni_{10}Al_{7.5}$
Force (gf)	Vickers Hardness (HV)		
25	429 ± 8	418 ± 10	425 ± 4
100	440 ± 7	430 ± 4	442 ± 3
2000	435 ± 4	398 ± 15	430 ± 14
Average	435 ± 6	415 ± 10	432 ± 7

transition from the pure Zr substrate to the printed BMG. When measured using 2000 gf, the hardness value of the LFP sample averages to 398 HV, which is lower than the value measured from the feedstock sheetmetal, which is 435 HV (Table 2). The Vickers hardness of 2 mm cast laboratory grade material is 430 HV, suggesting that the lower hardness of the LFP sample is a consequence of the porosity. Lowering the testing force, hence decreasing the interaction area and volume, results in hardness values that converges to the 430–440 HV range, concluding that the apparent decrease in hardness is the result of pores.

Four-point bending was used to evaluate the mechanical performance of the samples. Using a universal testing machine with a testing fixture such that the loading span is 1/3 the length of the support span, the flexural stress (σ_f) from four-point bending could be calculated using:

$$\sigma_f = \frac{FL}{bh^2}$$

where F is the force, L is the length of the support span, b is the sample width, and h is the sample height. Fig. 4 depicts the four-point bending measurements on 4.0 mm beams fabricated by LFP that were bent in the build direction and orthogonal to it. For all three samples, the beams yielded and deformed plastically prior to failure. The average flexural yield strength measured for all samples in this study is 1880 MPa. Although there was only a small sample size, the flexural strength was similar for all the tests, including the one done perpendicular to the build direction. Figs. 4d,e show optical micrographs of the printed sample after bending, showing a winding crack path and many shear bands on both the tension side and compression side. Of particular note is that the LFP sample has obvious porosity, which is normally a precursor to premature failure in an unconfined loading geometry, such as tension or bending. However, all three of the printed samples yielded and there is evidence of shear banding from the pores (Fig. 4d. inset).

Fig. 5b shows the results of the four-point bending tests that were performed on cast beams made from the remelted feedstock sheetmetal at 2.5, 3.5 and 4.5 mm (sample production outlined in Fig. 5a), regardless of the amount of crystallization. For the 3.5 and 4.5 mm beams, the sample has severely embrittled and only the 2.5 mm beams were ductile enough to yield and exhibit some bending plasticity. XRD measurements on the beams indicated that there is substantial crystallization for samples of at least 3.5 mm in size (Fig. 5c), whereas the 2.5 mm beam is fully amorphous, thus demonstrating that the LFP manufacturing process is able to produce BMG samples larger than the critical casting thickness of the sheetmetal alloy. The dramatic decrease in the GFA from remelting the feedstock sheetmetal, when compared to 16 mm attainable casting thickness in the literature [11], is a consequence of the impurities present in the commercial grade feedstock sheetmetal.

To determine the best possible mechanical properties attainable for $Zr_{65}Cu_{17.5}Ni_{10}Al_{7.5}$, laboratory grade material was fabricated and cast, which allows printed samples to be compared to a benchmark. Four-point bending experiments were performed on the square beams of thicknesses of 2.5, 3.5, 4.0, and 4.5 mm (Fig. 6). Despite BMGs normally categorized as being brittle materials, the results show that high-purity BMGs can have exceptional strength and toughness in bending. All of the sample sizes yielded (average flexural yield strength is 1880 MPa) and possessed significant bending plasticity, indicating superior mechanical properties and GFA as compared to industrial grade material at any sample dimension. The sample geometry affects the flexural modulus as well as the amount of plasticity present in the sample; thinner samples generally are less stiff and have higher bending plasticity. For the 4.0 mm thick samples, the same geometry as LFP samples (Fig. 4), it is clear that the cast laboratory grade samples outperformed the LFP samples due to the absence of porosity. However, it should be noted that even in the presence of porosity, LFP samples consistently display high strength and plasticity in bending, demonstrating the ability to produce BMG samples through AM with mechanical properties converging the benchmark set by cast laboratory grade material.

In addition to four-point bending tests, Vickers hardness was also measured between the sheetmetal feedstock, LFP samples, cast remelted sheetmetal, and cast laboratory grade material across multiple thicknesses (Fig. 7). The cast laboratory grade material have hardness values comparable to the value of the melt spun sheetmetal of 435 HV, which is indicative of the amorphous state. Beams cast from remelted sheetmetal that are 3.5 mm and larger are partially crystalline, indicated by the increase in hardness to 553 HV for the cast 3.5 and 4.5 mm beams. As mentioned above, the LFP samples show a reduced hardness due to the porosity present in the sample and the absence of crystallinity.

4. Summary and conclusions

BMGs can be produced in various feedstock forms that may be suitable for AM but limitations exist for each in terms of mass production scalability, cost, oxidation contamination risk, and usefulness for AM. The current work demonstrates the potential for achieving excellent mechanical properties from BMGs using additive manufacturing from a commercially manufactured feedstock, i.e. sheetmetal, which can be produced in large volumes with low oxygen content from a variety of alloys. Using BMG sheetmetal for LFP allows for continuously fed feedstock, leading to the ease of automation of the process. Although this work did not focus on the creation of net-shaped parts, as is common with much of the AM research, the focus was instead on measuring the mechanical properties of printed samples and then comparing them with samples made through conventional casting.

To summarize the findings, BMG samples produced with LFP demonstrated high strength and plastic strain in bending that greatly exceeded the properties of cast beams made from the identical remelted feedstock sheetmetal. Therefore, with the same BMG feedstock, LFP produced a superior sample to casting in terms of both GFA and bending plasticity. For the $Zr_{65}Cu_{17.5}Ni_{10}Al_{7.5}$ BMG alloy, which was selected due to the commercial availability of the sheetmetal, we determined the upper bound of the possible properties obtainable in the laboratory setting through vacuum suction casting ultra-high purity alloy, i.e. Hf-free with <100 ppm oxygen by weight, for mechanical testing. Despite BMGs normally considered to be brittle [1–3], we show that the laboratory grade alloy is excep-

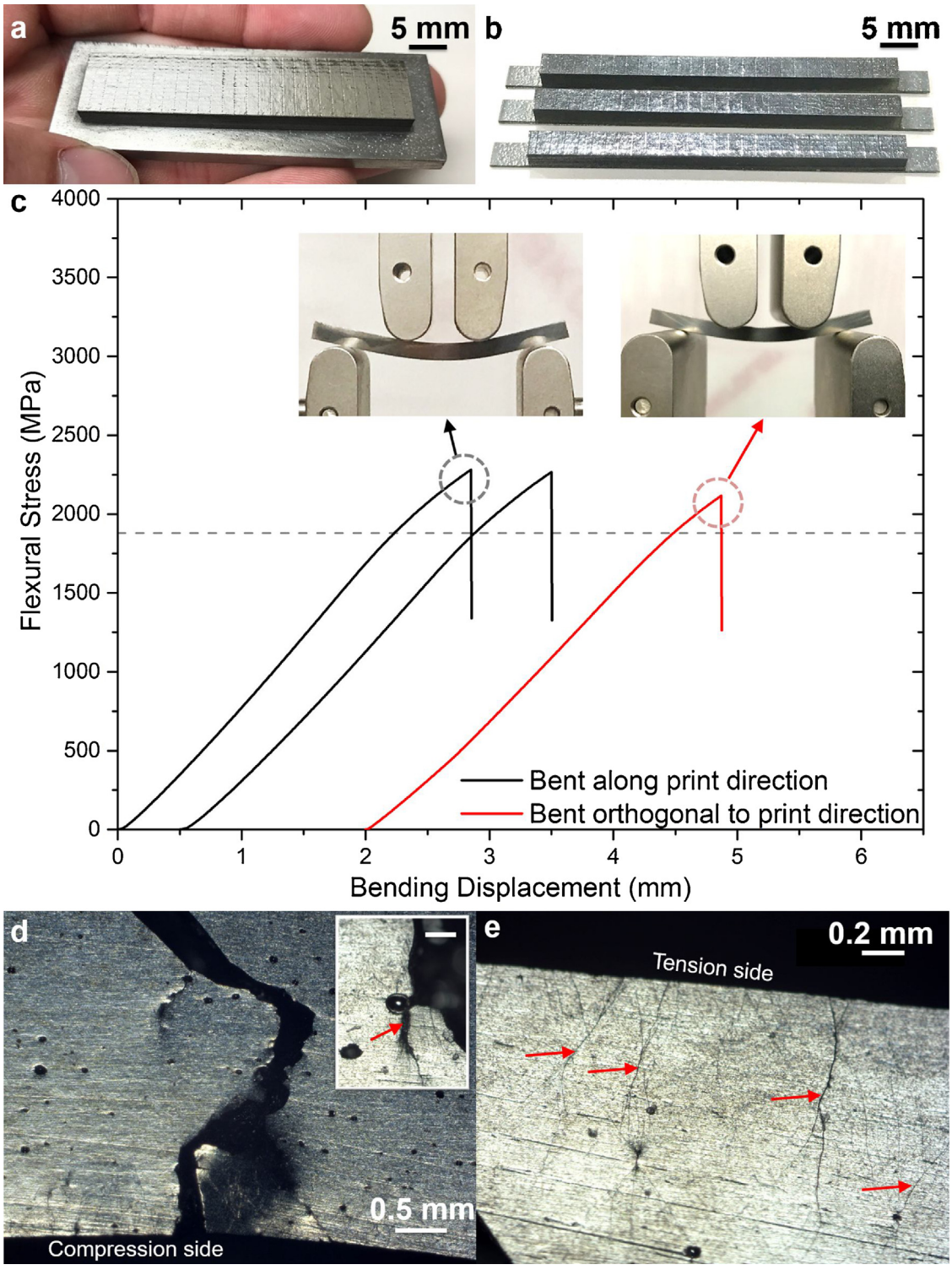

Fig. 4. Photographs of (a) the as-printed plate on a Zr substrate and (b) the beams post wire EDM, prior to grinding to a 4 mm square beam. (c) Results of four-point bending measurements on the laser foil printed beams. The dashed line is the average flexural yield strength of 1880 MPa. Insets are representative images of the beams prior to fracture. Optical micrograph of the fractured beam as viewed from the (d) compression side, near the fracture crack, and (e) tension side (fracture crack not shown). Inset is a zoomed in image of a pore. Scale bar is 100 μm. The scratches from the 600 grit SiC paper are in the direction longitudinal to the beam. Any evidence of shear bands is perpendicular to the beam's length. Arrows indicate the most prominent shear bands.

tional in four-point bending at all thickness that can be easily cast, up to 4.5 mm thick square beams. This demonstrates the potential for AM of BMGs if the feedstock fabrication, alloy purity, and manufacturing technology is improved. This work does not only show the promise of achieving similar properties to cast samples, but also demonstrates that AM can be extended to produce fully amorphous samples with thicknesses exceeding the critical casting thickness of the particular BMG. Despite the limits of the LFP technology for making high-resolution net-shapes, as is common with other AM techniques, the process is well-suited for making small billets of novel BMG alloys that can then be subsequently machined. In high-value applications, such as jewelry, gears, sensors, or mechanisms,

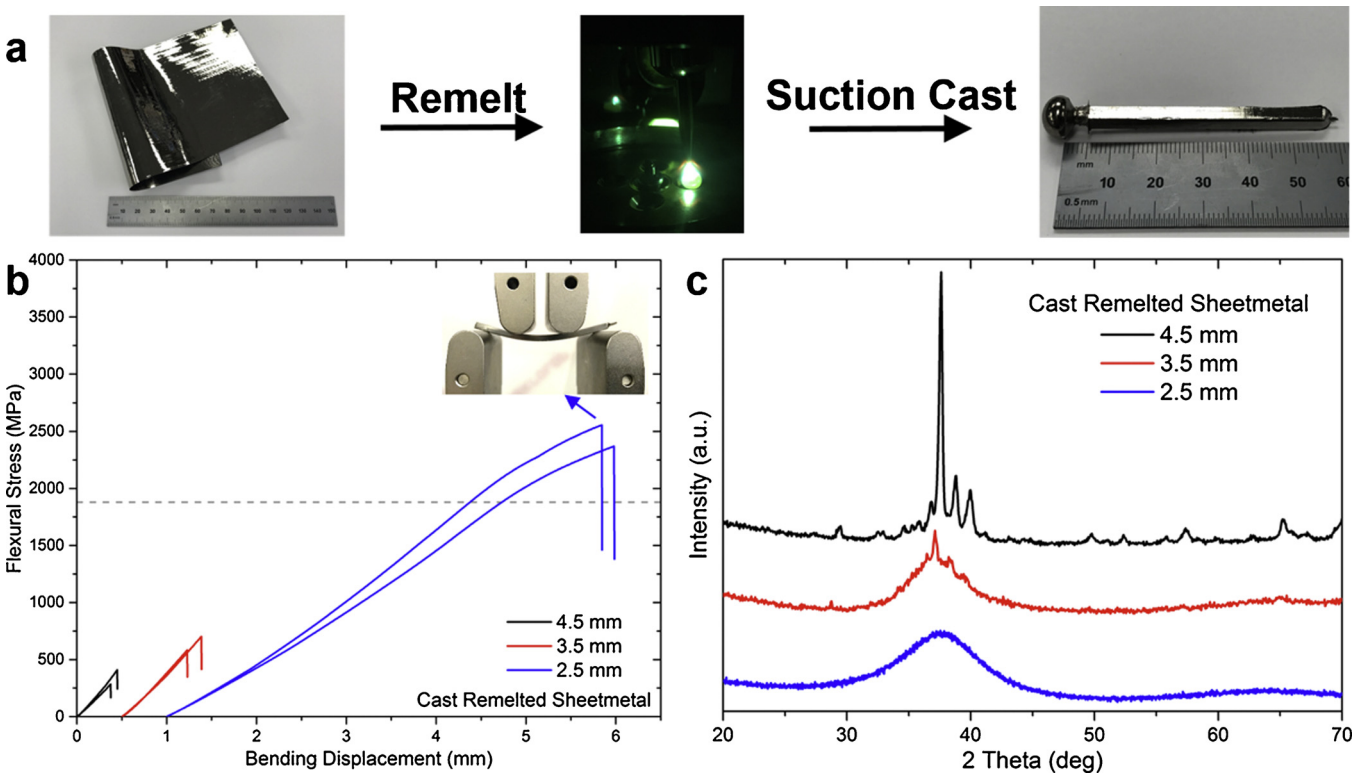

Fig. 5. (a) Flow chart describing the process by which the (left) feedstock sheetmetal is (center) carefully remelted in an arc melter and (right) suction cast to form beams for four-point bending. (b) Results of four-point bending measurements on beams cast from feedstock sheetmetal that was remelted. The inset shows a sample prior to fracture that has surpassed the yield point. The dashed line is the average flexural yield strength of 1880 MPa. (c) XRD measurements on the beams cast from remelted sheetmetal for different thicknesses.

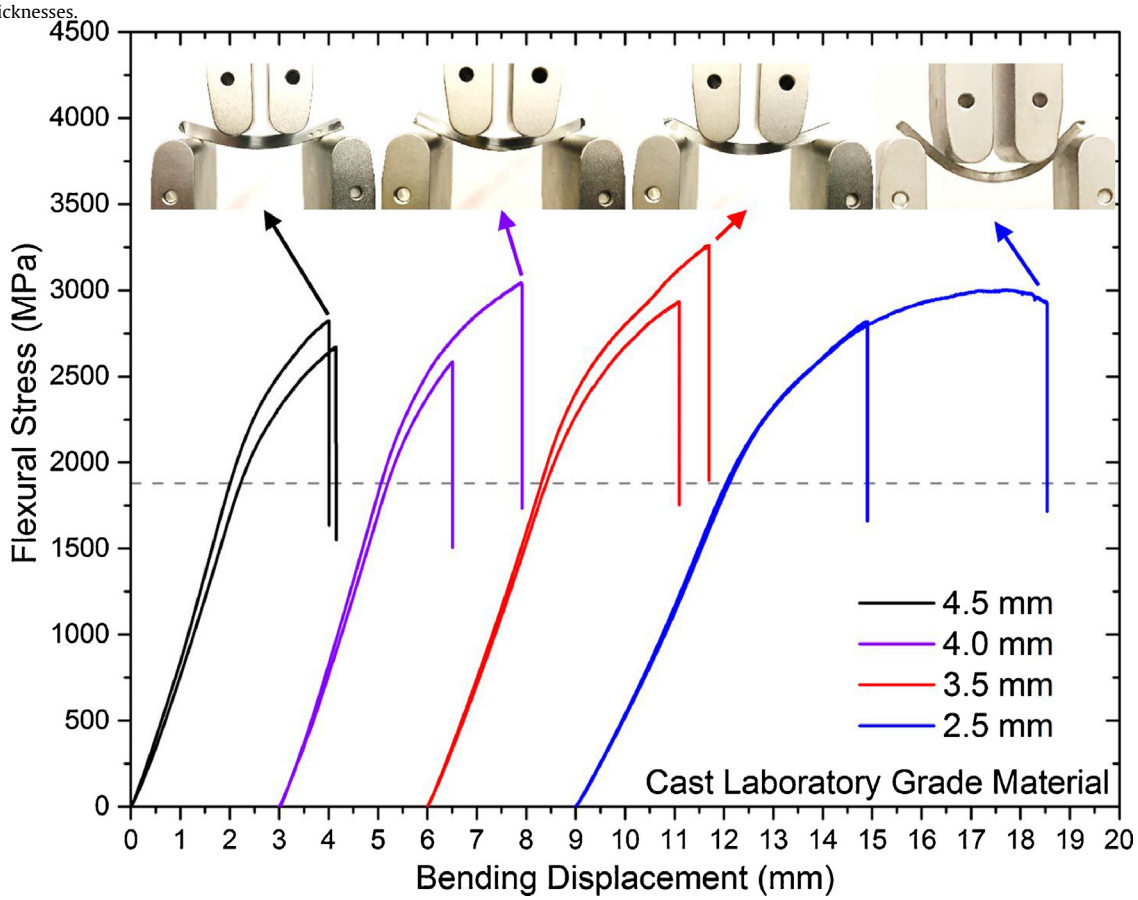

Fig. 6. Results of four-point bending measurements on beams cast from laboratory grade material. The insets show representative samples prior to fracture. The dashed line is the average flexural yield strength of 1880 MPa. At every dimension from the smallest that could be cast (2.5 mm) to the upper limit before the alloy crystallized (5 mm), bending plasticity was observed.

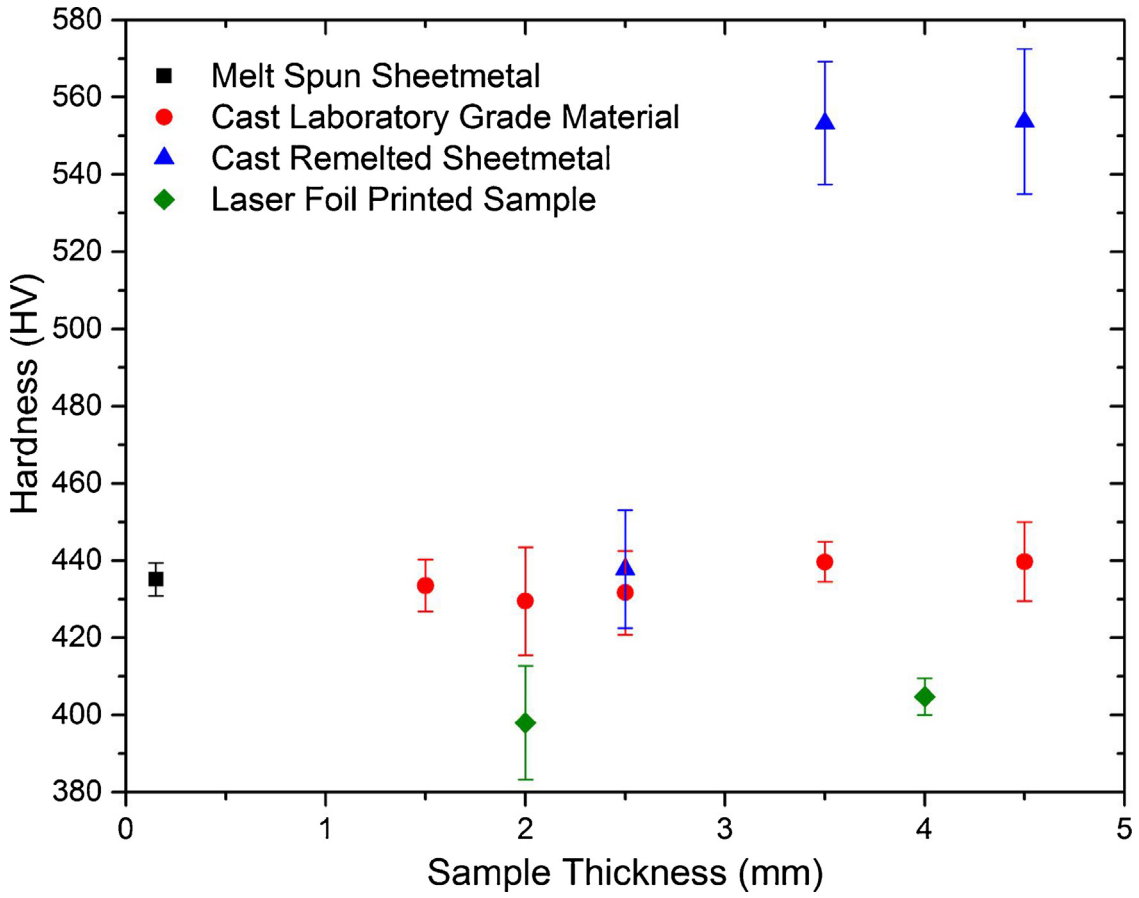

Fig. 7. Plot of the Vickers hardness measured at 2000 gf with a dwell time of 10 s versus the sample thickness of the melt spun sheetmetal, cast laboratory grade material, cast remelted melt spun sheetmetal, and samples produced via LFP.

the additional cost of machining the billet is overcome by the value of the BMG material properties in the intended application.

Future work will involve LFP using higher purity feedstock sheetmetal, including new alloys designed specifically for the process, such as precious metal or wear-resistant BMGs. The manufacturing will also be improved to better automate the process and produce net-shaped parts of interest. This work can also be extended to include tough composites and laminates.

Acknowledgements

Punnathat Bordeenithikasem's research was supported by an appointment to the NASA Postdoctoral Program at the NASA Jet Propulsion Laboratory, California Institute of Technology. The program is administered by Universities Space Research Association under contract with NASA. Douglas Hofmann acknowledges support from the Presidential Early Career Award. Part of this research was done at the NASA Jet Propulsion Laboratory, California Institute of Technology, under contract with NASA. The work at Missouri University of Science and Technology was supported by the Department of Energy (grant number DE-FE0012272).

References

[1] A.I. Salimon, M.F. Ashby, Y. Bréchet, A.L. Greer, Bulk metallic glasses: what are they good for? Mater. Sci. Eng. A 375–377 (2004) 385–388, http://dx.doi.org/10.1016/J.MSEA.2003.10.167.
[2] M.F. Ashby, A.L. Greer, Metallic glasses as structural materials, Scr. Mater. 54 (2006) 321–326, http://dx.doi.org/10.1016/J.SCRIPTAMAT.2005.09.051.
[3] M. Telford, The case for bulk metallic glass, Mater. Today 7 (2004) 36–43, http://dx.doi.org/10.1016/S1369-7021(04)00124-5.
[4] W.L. Johnson, Bulk glass-forming metallic alloys: science and technology, MRS Bull. 24 (1999) 42–56, http://dx.doi.org/10.1557/S0883769400053252.
[5] A. Peker, W.L. Johnson, A highly processable metallic glass: Zr 41.2 Ti 13.8 Cu 12.5 Ni 10.0 Be 22.5, Appl. Phys. Lett. 63 (1993) 2342–2344, http://dx.doi.org/10.1063/1.110520.
[6] J. Waniuk, Critical cooling rate and thermal stability of Zr–Ti–Cu–Ni–Be alloys, Appl. Phys. Lett. 78 (2001) 1213–1215, http://dx.doi.org/10.1063/1.1350624.
[7] A. Inoue, T. Zhang, T. Masumoto, Zr-Al-Ni amorphous alloys with high glass transition temperature and significant supercooled liquid region, mater, Trans. JIM 31 (1990) 177–183, http://dx.doi.org/10.2320/matertrans1989.31.177.
[8] T. Zhang, A. Inoue, T. Masumoto, Amorphous Zr-Al-TM (TM=Co, Ni, Cu) alloys with significant supercooled liquid region of over 100 K, Mater, Trans. JIM 32 (1991) 1005–1010, http://dx.doi.org/10.2320/matertrans1989.32.1005.
[9] Yoshihiko Yokoyama, Ductility improvement of Zr–Cu–Ni–Al glassy alloy, Non. Cryst. Solids 316 (2003) 104–113, http://dx.doi.org/10.1016/S0022-3093(02)01942-7.
[10] Y.J. Sun, D.D. Qu, Y.J. Huang, K.-D. Liss, X.S. Wei, D.W. Xing, J. Shen, Zr–Cu–Ni–Al bulk metallic glasses with superhigh glass-forming ability, Acta Mater. 57 (2009) 1290–1299, http://dx.doi.org/10.1016/J.ACTAMAT.2008.11.007.
[11] A. Inoue, T. Zhang, N. Nishiyama, K. Ohba, T. Masumoto, Preparation of 16 mm diameter rod of amorphous Zr65Al7.5Ni10Cu17.5, Alloy, Mater. Trans. JIM 34 (1993) 1234–1237, http://dx.doi.org/10.2320/matertrans1989.34.1234.
[12] D.C. Hofmann, L.M. Andersen, J. Kolodziejska, S.N. Roberts, J.-P. Borgonia, W.L. Johnson, K.S. Vecchio, A. Kennett, Optimizing bulk metallic glasses for robust, highly wear-resistant gears, Adv. Eng. Mater. 19 (2017) 1600541, http://dx.doi.org/10.1002/adem.201600541.
[13] D.C. Hofmann, R. Polit-Casillas, S.N. Roberts, J.-P. Borgonia, R.P. Dillon, E. Hilgemann, J. Kolodziejska, L. Montemayor, J.-O. Suh, A. Hoff, K. Carpenter, A. Parness, W.L. Johnson, A. Kennett, B. Wilcox, Castable bulk metallic glass strain wave gears: towards decreasing the cost of high-performance robotics, Sci. Rep. 6 (2016) 37773, http://dx.doi.org/10.1038/srep37773.
[14] J.-Z. Jiang, D. Hofmann, D.J. Jarvis, H.-J. Fecht, Low-density high-strength bulk metallic glasses and their composites: a review, Adv. Eng. Mater. 17 (2015) 761–780, http://dx.doi.org/10.1002/adem.201400252.
[15] W.L. Johnson, Bulk amorphous metal—an emerging engineering material, JOM 54 (2002) 40–43, http://dx.doi.org/10.1007/BF02822619.

[16] J. Schroers, Processing of bulk metallic glass, Adv. Mater. 22 (2010) 1566–1597, http://dx.doi.org/10.1002/adma.200902776.
[17] E.R. Homer, M.B. Harris, S.A. Zirbel, J.A. Kolodziejska, H. Kozachkov, B.P. Trease, J.-P.C. Borgonia, G.S. Agnes, L.L. Howell, D.C. Hofmann, New methods for developing and manufacturing compliant mechanisms utilizing bulk metallic glass, Adv. Eng. Mater. 16 (2014) 850–856, http://dx.doi.org/10.1002/adem.201300566.
[18] P. Bordeenithikasem, S. Sohn, Z. Liu, J. Schroers, Protocols for multi-step thermoplastic processing of metallic glasses, Scr. Mater. 104 (2015) 56–59, http://dx.doi.org/10.1016/j.scriptamat.2015.03.024.
[19] J. Ketkaew, Z. Liu, W. Chen, J. Schroers, Critical crystallization for embrittlement in metallic glasses, Phys. Rev. Lett. 115 (2015) 265502, http://dx.doi.org/10.1103/PhysRevLett.115.265502.
[20] R.O. Gilbert, W.L. Ritchie, Fracture toughness and fatigue-crack propagation in a Zr–Ti–Ni–Cu–Be bulk metallic glass, Appl. Phys. Lett. (1998), http://dx.doi.org/10.1063/1.119610.
[21] P. Bordeenithikasem, J. Liu, S.A. Kube, Y. Li, T. Ma, B.E. Scanley, C.C. Broadbridge, J.J. Vlassak, J.P. Singer, J. Schroers, Determination of critical cooling rates in metallic glass forming alloy libraries through laser spike annealing, Sci. Rep. 7 (2017) 7155, http://dx.doi.org/10.1038/s41598-017-07719-2.
[22] Y. Shen, Y. Li, C. Chen, H.-L. Tsai, 3D printing of large, complex metallic glass structures, Mater. Des. 117 (2017) 213–222, http://dx.doi.org/10.1016/j.matdes.2016.12.087.
[23] S. Pauly, L. Löber, R. Petters, M. Stoica, S. Scudino, U. Kühn, J. Eckert, Processing metallic glasses by selective laser melting, Mater. Today 16 (2013) 37–41, http://dx.doi.org/10.1016/j.mattod.2013.01.018.
[24] B. Zheng, Y. Zhou, J.E. Smugeresky, J.M. Schoenung, E.J. Lavernia, Thermal behavior and microstructural evolution during laser deposition with laser-engineered net shaping: part I. Numerical calculations, Metall. Mater. Trans. A 39 (2008) 2228–2236, http://dx.doi.org/10.1007/s11661-008-9557-7.
[25] W.E. Frazier, Metal additive manufacturing: a review, J. Mater. Eng. Perform. 23 (2014) 1917–1928, http://dx.doi.org/10.1007/s11665-014-0958-z.
[26] K.V. Wong, A. Hernandez, A review of additive manufacturing, ISRN Mech. Eng. 2012 (2012) 1–10, http://dx.doi.org/10.5402/2012/208760.
[27] J.J. Lewandowski, M. Seifi, Metal additive manufacturing: a review of mechanical properties, Annu. Rev. Mater. Res. 46 (2016) 151–186, http://dx.doi.org/10.1146/annurev-matsci-070115-032024.
[28] A. Jabbari, K. Abrinia, A metal additive manufacturing method: semi-solid metal extrusion and deposition, Int. J. Adv. Manuf. Technol. (2017) 1–10, http://dx.doi.org/10.1007/s00170-017-1058-7.
[29] D. Ding, Z. Pan, D. Cuiuri, H. Li, Wire-feed additive manufacturing of metal components: technologies, developments and future interests, Int. J. Adv. Manuf. Technol. 81 (2015) 465–481, http://dx.doi.org/10.1007/s00170-015-7077-3.
[30] M. Agarwala, D. Bourell, J. Beaman, H. Marcus, J. Barlow, Direct selective laser sintering of metals, Rapid Prototyp. J. 1 (1995) 26–36, http://dx.doi.org/10.1108/13552549510078113.
[31] E. Williams, N. Lavery, Laser processing of bulk metallic glass: a review, J. Mater. Process. Technol. 247 (2017) 73–91, http://dx.doi.org/10.1016/J.JMATPROTEC.2017.03.034.
[32] S. Pauly, C. Schricker, S. Scudino, L. Deng, U. Kühn, Processing a glass-forming Zr-based alloy by selective laser melting, Mater. Des. 135 (2017) 133–141, http://dx.doi.org/10.1016/j.matdes.2017.08.070.
[33] X.P. Li, M.P. Roberts, S. O'Keeffe, T.B. Sercombe, Selective laser melting of Zr-based bulk metallic glasses: processing, microstructure and mechanical properties, Mater. Des. 112 (2016) 217–226, http://dx.doi.org/10.1016/j.matdes.2016.09.071.
[34] H.Y. Jung, S.J. Choi, K.G. Prashanth, M. Stoica, S. Scudino, S. Yi, U. Kühn, D.H. Kim, K.B. Kim, J. Eckert, Fabrication of Fe-based bulk metallic glass by selective laser melting: a parameter study, Mater. Des. (2015), http://dx.doi.org/10.1016/j.matdes.2015.07.145.
[35] H. Sun, K.M. Flores, Laser deposition of a Cu-based metallic glass powder on a Zr-based glass substrate, J. Mater. Res. 23 (2008) 2692–2703, http://dx.doi.org/10.1557/JMR.2008.0329.
[36] H. Sun, K.M. Flores, Microstructural analysis of a laser-processed Zr-based bulk metallic glass, Metall. Mater. Trans. A 41 (2010) 1752–1757, http://dx.doi.org/10.1007/s11661-009-0151-4.
[37] P. Tsai, K.M. Flores, High-throughput discovery and characterization of multicomponent bulk metallic glass alloys, Acta Mater. 120 (2016) 426–434, http://dx.doi.org/10.1016/j.actamat.2016.08.068.
[38] P. Tsai, K.M. Flores, A laser deposition strategy for the efficient identification of glass-forming alloys, Metall. Mater. Trans. A 46 (2015) 3876–3882, http://dx.doi.org/10.1007/s11661-015-2900-x.
[39] Y. Li, Y. Shen, C. Chen, M.C. Leu, H.-L. Tsai, Building metallic glass structures on crystalline metal substrates by laser-foil-printing additive manufacturing, J. Mater. Process. Technol. 248 (2017) 249–261, http://dx.doi.org/10.1016/j.jmatprotec.2017.05.032.
[40] J. Dowden, N. Postacioglu, M. Davis, P. Kapadia, A keyhole model in penetration welding with a laser, J. Phys. D. Appl. Phys. 20 (1987) 36–44, http://dx.doi.org/10.1088/0022-3727/20/1/006.
[41] W. Chen, H. Zhou, Z. Liu, J. Ketkaew, N. Li, J. Yurko, N. Hutchinson, H. Gao, J. Schroers, Processing effects on fracture toughness of metallic glasses, Scr. Mater. 130 (2017) 152–156, http://dx.doi.org/10.1016/j.scriptamat.2016.11.011.
[42] V. Keryvin, C. Bernard, J.-C. Sanglebœuf, Y. Yokoyama, T. Rouxel, Toughness of Zr55Cu30Al10Ni5 bulk metallic glass for two oxygen levels, J. Non. Cryst. Solids 352 (2006) 2863–2868, http://dx.doi.org/10.1016/j.jnoncrysol.2006.02.102.
[43] Y. Yokoyama, A. Kobayashi, K. Fukaura, A. Inoue, Oxygen embrittlement and effect of the addition of Ni element in a bulk amorphous Zr-Cu-Al alloy, Mater. Trans. 43 (2002) 571–574, http://dx.doi.org/10.2320/matertrans.43.571.
[44] J. Eckert, N. Mattern, M. Zinkevitch, M. Seidel, Crystallization behavior and phase formation in Zr-Al-Cu-Ni metallic glass containing oxygen, mater, Trans. JIM 39 (1998) 623–632, http://dx.doi.org/10.2320/matertrans1989.39.623.
[45] Z.P. Lu, H. Bei, Y. Wu, G.L. Chen, E.P. George, C.T. Liu, Oxygen effects on plastic deformation of a Zr-based bulk metallic glass, Cit. Appl. Phys. Lett. 92 (2008), http://dx.doi.org/10.1063/1.2828981.
[46] X.H. Lin, W.L. Johnson, W.K. Rhim, Effect of oxygen impurity on crystallization of an undercooled bulk glass forming Zr-Ti-Cu-Ni-Al alloy, Mater. Trans. JIM 38 (1997) 473–477, http://dx.doi.org/10.2320/matertrans1989.38.473.